



## Research Article

# Effect of solid solution phase constitution on dissimilar Al/Cu FSW using Zn as an alloying element at the joint interface

Prakash Kumar Sahu<sup>1</sup> · Sukhomay Pal<sup>2</sup> · Qingyu Shi<sup>1</sup>

Received: 8 October 2019 / Accepted: 15 November 2019 / Published online: 22 November 2019  
© Springer Nature Switzerland AG 2019

## Abstract

The effect of Al/Zn/Cu binary and ternary solid solution phase constituents on metallurgical and mechanical properties of Al/Cu dissimilar friction stir welding using Zn as an alloying element was investigated. Because of Zn interlayer material binary intermetallic compounds (IMCs) such as AlCu, Al<sub>2</sub>Cu, Al<sub>71</sub>Zn<sub>29</sub>, CuZn<sub>5</sub> and ternary IMCs such as Al<sub>4.2</sub>Cu<sub>3.2</sub>Zn<sub>7</sub> are formed. These solid solution alloying phase constituents improved the weld properties of the joint. The tensile strength was enhanced by 13% for Zn alloying specimens compared with non-alloyed weld specimen and 104% of the Al base material due to the formation of thin and controlled IMCs and solid solution phase constitution strengthening as well as Orowan strengthening. The fractured surface with Zn alloying element suggested combination of ductile–brittle fracture and indicated transgranular failure. Micro-hardness with Zn alloying specimen is higher compared to the non-alloyed specimen for the existence of different IMCs at the stir-zone. The mapping analysis indicated that the thickness of the IMCs with Zn alloying was at micro-meter level. Phase constituent revealed that thin continuous and uniformly distributed binary and ternary phases are beneficial for the enhancement of mechanical and metallurgical qualities. Macrostructural views revealed variation in IMCs flows at non-alloyed and Zn alloying cases. Different weld zone reflected grain variations and finer grain at the weld nugget due to the nucleating effect of Zn interlayer.

**Keywords** Dissimilar FSW · Interlayer alloying · Phase constituents · Macro/microstructural analysis · Mechanical properties

## 1 Introduction

Dissimilar fusion welding of Al/Cu forms different intermetallic compounds (IMCs) with high hardness and brittleness at the joint interface. Non-uniform distribution and non-homogeneity of IMCs in the weld zone are major causes of formation of micro-cracks [1] and pores [2] as well as deterioration of weld quality. The IMCs are also formed in dissimilar friction stir welding (FSW) process [2, 3]. However a uniform distribution is achieved because of constant stirring of the weld nugget by the FSW tool. Moreover, preventing the formation of excess IMCs in the

Al/Cu weld is highly desirable to enhance the mechanical properties. Proper alloying using a third material can also be adopted in dissimilar joining to enhance the mechanical properties. The application of suitable alloying material at the faying zone of the joining plates can control the IMCs formation. Published research articles indicate that IMCs is the main source of reinforcing [4] in dissimilar welding. Hence, the developments of precise amount of intermetallic and uniform distribution of IMCs are the key factors for getting enhanced mechanical properties. These can be achieved by using a suitable alloying material as a third element at the weld interface.

✉ Qingyu Shi, shqy@mail.tsinghua.edu.cn; Prakash Kumar Sahu, prakashsahu.besu@gmail.com; Sukhomay Pal, spal@iitg.ac.in |  
<sup>1</sup>Department of Mechanical Engineering and IDM Joint Lab, Tsinghua University, Beijing 100084, China. <sup>2</sup>Department of Mechanical Engineering, Indian Institute of Technology Guwahati, Guwahati, Assam 781039, India.



There are few research articles that study the dissimilar Al/Cu FSW with third material as alloying elements. Akbari et al. [1] investigated Al/Cu lap FSW using Cu anodized Al plate to prevent the IMCs formation. Kuang et al. [3] also investigated Al/Cu dissimilar FSW using Zn as an interlayer in between Al and Cu at the lap joint surface to understand its effect on mechanical properties using a pin less tool. Boucherit et al. [5] used Zn interlayer in Al/Cu dissimilar friction stir spot welding process and observed that Zn hinders the formation of brittle IMCs and enhances the weld properties. However, the number of research works is very limited in Al/Cu dissimilar FSW compared to wide research works of Al alloy and other similar and dissimilar alloys. It is also observed that most of the researchers considered lap joint configuration using Zn element. The investigation of the butt joint configuration is rare. Other than the Al/Cu FSW with Zn as third material, researchers also studied on different materials with different alloying element using FSW as well as other welding processes. Kandasamy et al. [6] conducted dissimilar Al alloys plates FSW with Cu as intermediate inclusion in the form of strip, granules and coating at the faying surface to improve weld strength. Shiri et al. [7] examined the dispersal phenomenon of Al plate with insertion of thin Cu foil as well as a pure Zn foil to influence the mechanical properties. Aonuma et al. [8] studied the effect of Al content in different grade of Mg alloy (AZ31, AZ61 and AZ91) to weld with Ti alloy and observed that the tensile strength of joint deteriorate with increasing Al content. They [9] also worked on different grade of Mg (AMCa602, AM60 variation of Ca %) weld with Ti alloy and resulted in higher tensile strength in case of Ca content. Balasundaram et al. [2] experimented on Al/Cu joining with Zn interlayer by ultrasonic spot welding method to enhance mechanical and microstructural properties of the joint. Zheng et al. [10] used Zn filler metal in Al and steel, lap FSW and observed better strength compared to without filler metal. Ratanathavorn et al. [11] also observed that Zn interlayer enhanced the mechanical strength in Al/steel lap FSW.

This investigation is for detailed understanding of the effect of alloying element at the joint interface in the form of solid solution phase constituent. Zn was chosen as the interlayer alloying material in the form of thin metallic foil. The thin foil was introduced at faying edges of the plates and believed that it will enhance the mechanical properties by the formation of solid solution phases. The current technique is innovative and it is first try of using Zn alloying foil in Al/Cu butt joint FSW. In Al/Cu FSW, the process temperature at the weld nugget could reach above 450 °C. At this temperature Zn foil can melt (Zn melting point is 419.5 °C) and behave as an alloying component at the faying surface and it may enhance the mechanical properties. The Zn is selected for alloying element because of better

reaction feasibility with Al/Cu and formation of favorable binary and ternary compounds as observed in the phase diagram [12]. The present investigation is mainly focusing on the effect of solid solution phase constituent and exploring enhancement of the weld qualities using Zn third material as an alloying element.

## 2 Experimental details

The FSW experiment was conducted on 1050 aluminium alloy (AA) and Cu alloy in single pass butt joint configuration. The workpiece plate dimension is 150 mm × 100 mm × 4 mm. The measured elemental composition, in wt.%, of AA1050 is Fe-0.40%, Si-0.25%, Zn-0.07% and Mn, Mg, Cu, Ti, each of 0.05% and the remaining is Al. The Cu elemental composition is 0.02% Ag, and Zn, Sn, Fe, Cr, Ni, Zr, P, Pb each of 0.005% and remaining is Cu. Table 1 indicates the tested mechanical properties of the Cu and Al base plates. The Al and Cu workpieces were put on the retreating and the advancing side of the rotating tool, respectively. An optimized tool offset of 1.5 mm was given towards the soft Al alloy for proper weld qualities [13]. The tool material used is H13 steel and fabricated cylindrical pin of 6 mm diameter, 25 mm shoulder diameter and 3.5 mm pin length. The details of the experimental conditions are shown in Table 2. The thickness of the Zn interlayer material was 0.4 mm and placed in-between the Al and Cu plates along the weld line.

After the completion of experiments, three tensile samples, one sample each for hardness and microstructure investigation were taken out from each welded specimen. The average of three tensile results was considered for the final investigation. The weld attributes namely, ultimate tensile strength (UTS), elongation percentage, micro-hardness (HV) of the weld nugget zone (NZ), macro and microstructural features were considered from each sample. The tensile test was performed by using a Dynamic UTM machine according to ASTM E8M04 guideline. The percentage of elongation was measured using 50 mm gauge length extension meter. The hardness value of each specimen was measured using a Vickers indenter at 300 g pressure and dwell time of 10 s. The macro and microstructures were taken after chemical etching. The Al weld surface was

**Table 1** Mechanical attributes of the received base metal

Base materials	Yield strength (MPa)	Ultimate tensile strength (MPa)	Percentage of elongation	Micro-hardness value (HV)
AA1050	119	132	12	43
Cu alloy	190	206	27	71

**Table 2** Experimental conditions

Experiment no.	Welding speed (mm/min)	Plunge depth (mm)	Interlayer	Tool rotational speed (rev/min)
E1	30	0.1	Without interlayer	600
E2				1200
E3				1800
E4				2400
EZn1	30	0.1	With Zn interlayer	600
EZn2				1200
EZn3				1800
EZn4				2400

etched using Keller's solution and Cu weld surface using 10 ml ethanol, 5 g  $\text{FeCl}_3$  and HCl 10 ml added to distilled water 50 ml. Analysis of phase constituent of the extracted samples against each experiment was accomplished by field emission scanning electron microscope (FESEM). EDX analysis was performed by using the same FESEM connected with EDX test setup. Element dispersal of the corresponding sample was detected by FESEM furnished with element map and line scan technique. The detected substance composition using EDX technique was established by X-ray diffraction (XRD) technique.

### 3 Results and discussion

This section mainly reveals the effect of metallurgical and mechanical properties due to the presence of binary and ternary solid solution phase constituents, those are formed by the Zn alloying element at the interface of Al/Cu joint. Macro and microstructural investigation of the weld is also achieved to study the bead geometry and grain size at different zones.

#### 3.1 Weld surface morphology and weld bead geometry

Figure 1 shows the appearance of the top surface and cross-section of the welds at various tool rotation speeds for both with and without Zn alloying cases. Figure 1a,

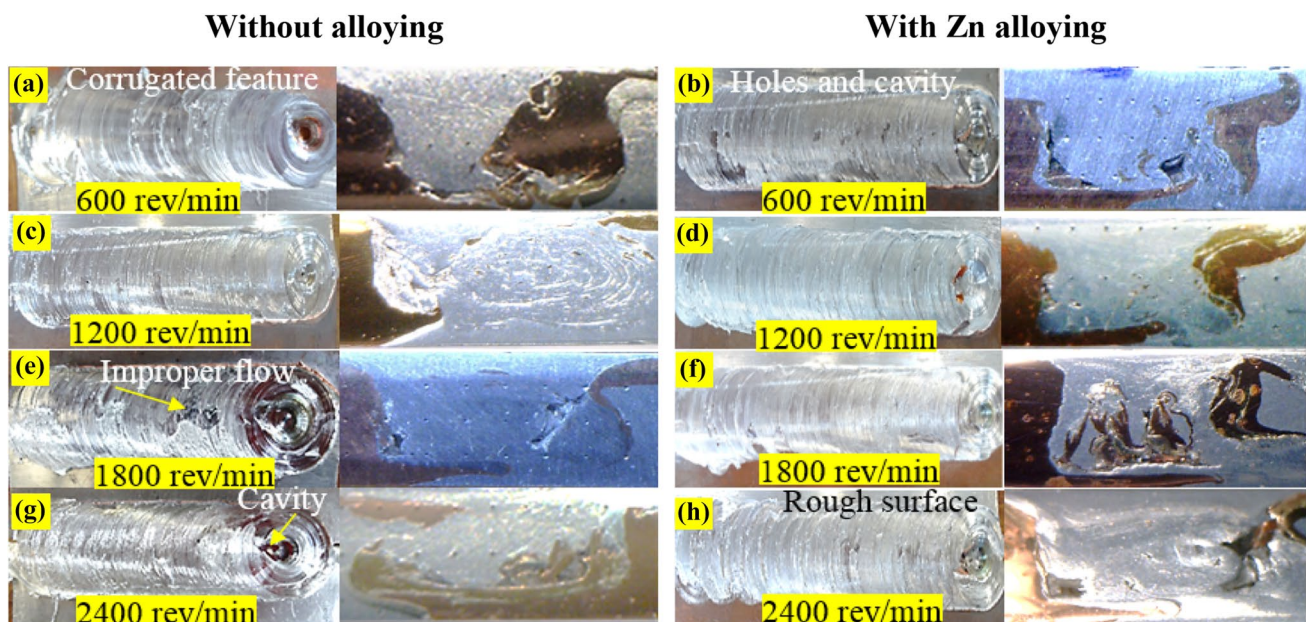


**Fig. 1** Various features of weld bead top surface and weld bead cross-section at different tool rotation speed for Zn alloying and non-alloying cases

shows corrugated features with apparent ripples on the top surface of weld bead. This is because of insufficient heat generation at 600 rev/min tool rotational speed. The similar appearance was also observed with Zn interlayer at the same parameter setting, as represented in the Fig. 1b. There are some holes and cavities which deteriorate the weld qualities. Figure 1c, d show, bead geometry for 1200 rev/min rotational speed. It is seen that the appearance of the top surface is smooth and without defects such as voids and flash. This may be due to proper heat generation at this speed. The superior mechanical properties are also found in this case, details are presented in the next section.

The local thinning with improper material flow beneath the shoulder surface is observed at 1800 rev/min tool rotation speed, shown in the Fig. 1e, f. Since more heat is generated at higher rotational speed that facilitates plasticized material to expelled out form the weld zone. Similarly, at 2400 rev/min, thinnest weld bead with cavity defect (Fig. 1g) were observed for the welded sample without alloying element because of higher heat generation. Whereas, inconsistent material flow and rough surface are observed in the Zn alloying sample (Fig. 1h). At higher tool rotation speed more amount of Cu is plasticized and mixed with Al by the stirring action of the tool. However, these Cu particles do not melt during the FSW process and the undissolved Cu creates faint burr and rough surface. In terms of surface quality, the weld at 1200 rev/min is the most satisfying appearance and without imperfection in the cross sectional view. However, it needs further investigation to differentiate weld strength as well as microstructure for various welding cases. The weld quality, as discussed in next section, reveal that the sample welded at 1200 rev/min exhibited highest weld strength compared to other tool rotational speeds. Therefore, the outcome of the solid solution

phase constituents only for the samples welded at 1200 rev/min is presented.

### 3.2 Tensile properties and micro-hardness distribution

In this section, ultimate tensile strength and percentage of elongation of the extracted tensile specimens are evaluated. Micro-hardness of the extracted specimens is also presented in detail for without alloying and with Zn alloying experiments. It was witnessed that the tensile fracture occurs at NZ or at NZ/TMAZ interface on the Al as well as Cu sides as shown in the Fig. 2a. The stress versus strain curves for the specimen of non-alloying E2 and Zn alloying EZn2 are represented in Fig. 2b. These specimens are considered as they are having highest ultimate tensile strength. It was detected that the tensile strength of sample E2 is 126.03 MPa which is around 95% of the Al base material and in case of specimen with Zn alloying, EZn2, is 142.29 MPa which is around 108% of Al base material and 69% of Cu base metal. The sample EZn2 strength is further than 100% compared to Al base material is because of the reinforcement of the phase constitution [4] and uniform distribution of IMCs. This may also due to proper diffusion [4], thin and controlled formation of IMCs [6] and the formation of solid solution phase constitution strengthening [14, 15]. The comparable reinforcement effect was also detected by other researchers [4, 6]. The effect of this strengthening is contributed from composite structure, fine grains at the stir zone and Orowan strengthening [16] effect for the dispersed IMCs. The phase constituent  $Al_{.71}Zn_{.29}$  also helped in improving the tensile strength.

The effect of tool rotation speed on ultimate tensile strength and percentage of elongation, in case of without alloying and with Zn interlayer alloying is represented in Fig. 2c. It was witnessed that when the tool rotation varies from 600 to 1200 rev/min, the strength as well as

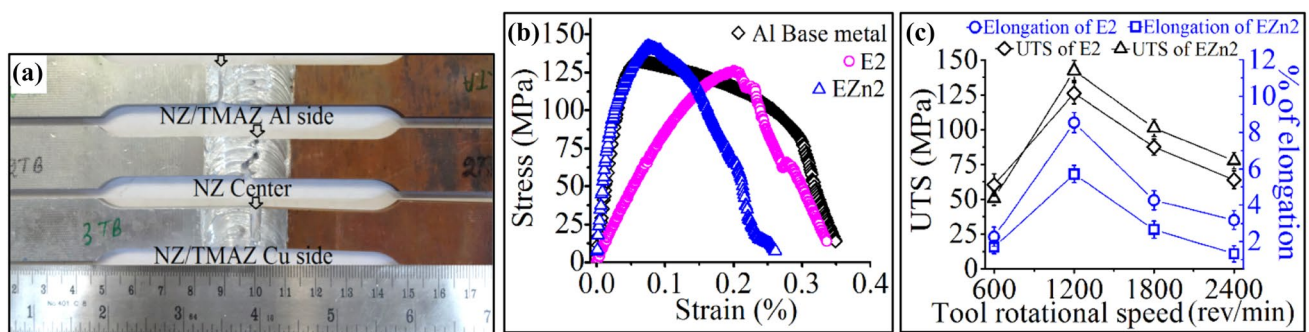


**Fig. 2** a Tensile tested specimens representing fracture at NZ/TMAZ interface of Al side, NZ center and NZ/TMAZ interface of Cu side, b stress versus strain curves for specimens E2, EZn2 and Al

base metal, c variation of UTS and % of elongation for without and with alloy at different tool rotation speed

percentage of elongation also increase due to an adequate friction heat generation that leads to proper joint. However, further increase in the tool rotation speed, the same attributes are in declining trend. Although, the plunging depth, welding speed and tool offset were kept constant throughout the experiment. During welding, it was observed that more amount of flash was generated surrounding to the tool shoulder in the retreating side. This flash causes local thinning that deteriorates the strength at high temperature due to higher tool rotational speed. On the other hand, at higher heat input, overlapped IMCs layer may develop that leads to quick crack beginning and deteriorates the tensile strength. It was also detected that the sample EZn2 gives more strength compared to sample E2 at 1200 rev/min because of the uniform and thin phase constitution distribution. The existent of binary phase  $Al_{71}Zn_{29}$  and ternary phase  $Al_{4.2}Cu_{3.2}Zn_{7.7}$  around the edges of the joint improves the weld strength. However, opposite phenomenon is observed in percentage elongation. Due to the development of extra IMCs like  $CuZn_5$  and ductility of the joint deteriorates.

Hardness of the welded specimens was measured at the bottom, middle and upper weld zones, shown in Fig. 3a. A total of 20 micro-hardness values were taken at an interval of 1 mm at the NZ and an interval of 2 mm at the TMAZ and heat affected zone (HAZ). The hardness of the bottom zone is higher than that of middle and upper zones due to more precipitation of IMCs in the bottom zone as represented in the Fig. 3b. It was also observed that the micro-hardness at the nugget zone is significantly more due to the presence of different phase constituents and finer grains [17, 18] compared to TMAZ, HAZ and BM as revealed in Fig. 3c. The actual indentation profile is shown in Fig. 3b to differentiate the indentation size and the hardness value due to the formation of various phase constituents in the form of IMCs. It was observed that the indentation size of the unreacted Cu part is larger with a hardness value of 71 HV but on the Al side due to formation of finer IMCs the indentation size is less and hardness is 115 HV. However, smallest indentation is observed at the

bottom with highest hardness value of 206 HV due to the presence of Al/Cu/Zn ternary phase constituent. The variation of hardness value at the bottom zone of the specimen E2 and EZn2 is represented in the Fig. 3c. It was detected that non-alloying joint bears less hardness compared to Zn alloying case because of the formation of ternary phase constitution. The maximum hardness in case of E2 was 176.2 HV however EZn2 indicated 206 HV.

### 3.3 Material flow and macrostructural variation

An appropriate mixing of Al and Cu base materials during friction stir process can produce reliable and defect free joint. Improper mixing can lead to the formation of unfavorable IMCs which deteriorate the weld quality. The macrostructure of material flow at various tool rotational speeds is revealed in the Fig. 4. In all the samples it was detected that Cu fragments were dispersed in Al matrix. It was also observed that the Cu particles were properly mixed with Al and formed different binary compound for without alloying element cases as revealed in the Fig. 4c, e at 1200 and 1800 rev/min tool rotation, respectively. These figures revealed that fine Cu particles are distributed over the Al matrix and produced stirring ring pattern composite structure which is beneficial for the enhancement of mechanical properties. However, Al/Zn/Cu binary and ternary IMCs are generated in case of Zn alloying at the weld area as shown in the Fig. 4d, f. These IMCs are uniformly distributed over a narrow region compared to the non-alloying case. The thin layer of IMCs flows in the direction of stirring pin.

The formed IMCs are associated with rotation behavior leads to a depth of intermixing with the base matrix. As well as the extrusion effect of stirring pin leading to fine mixing of IMCs into the base. The weld at 1200 rev/min, as shown in the Fig. 4c, d, shows defect free joint. The Cu fragment of various sizes and shapes in the form of binary IMCs are distributed uniformly over the Al matrix. In the case of Zn alloying element, the binary and ternary compounds are denser and uniform which

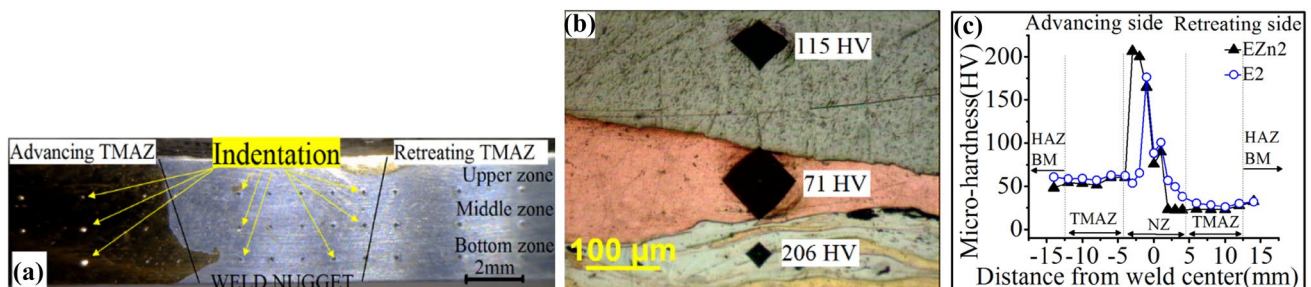
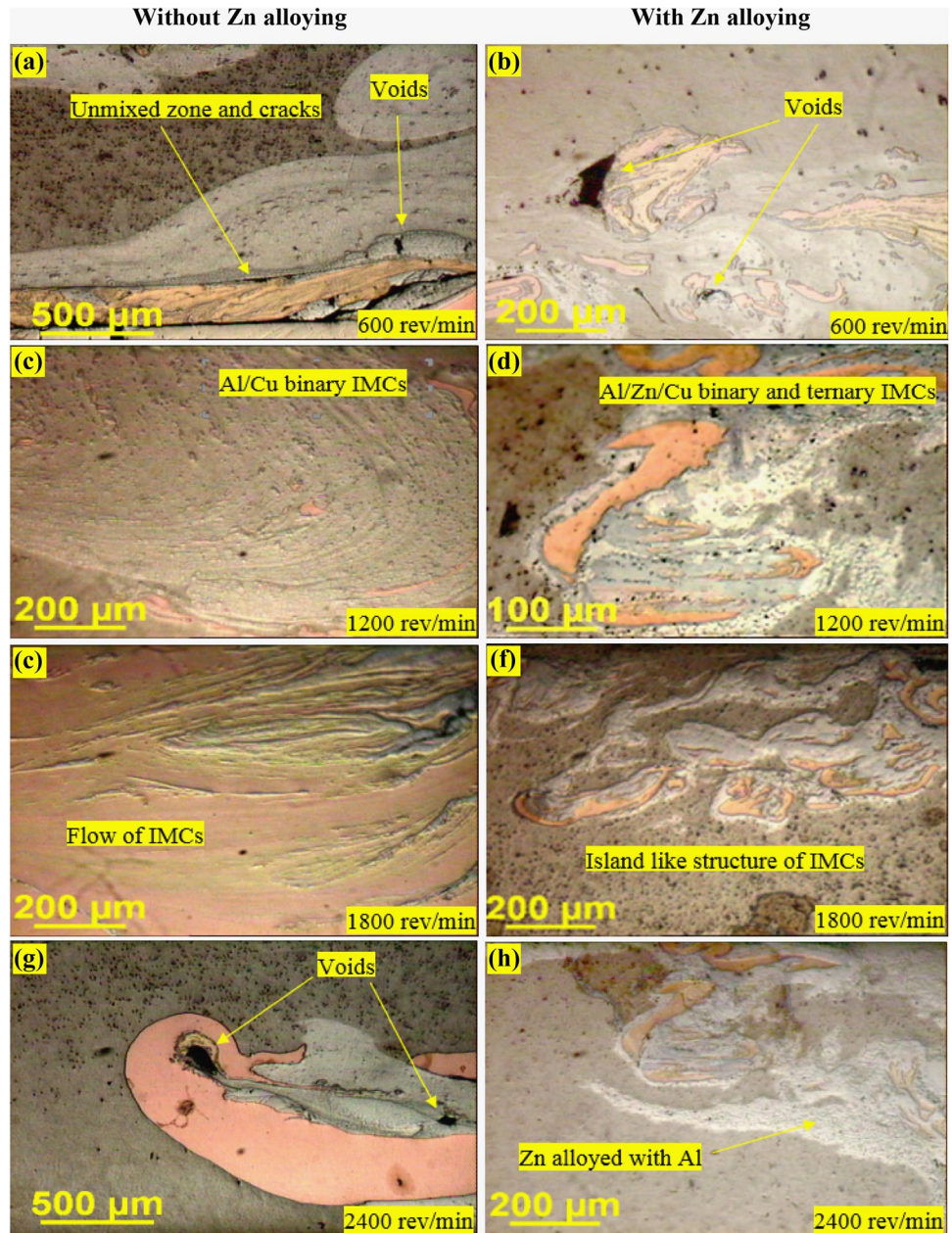


**Fig. 3** **a** Indentation profile of weld cross-section, **b** macrograph indentation at different zone and **c** comparison of micro-hardness in case of E2 and EZn2

**Fig. 4** The material flow at different tool rotation speeds for both with and without Zn alloying element



may lead to better mechanical properties. Figure 4a, b shows voids and large size unbroken Cu particles without proper mixing due to insufficient heat generation at 600 rev/min. At lower tool rotation speed the fragmented Cu is in bulk size and having less kinematic viscosity. Due to less viscosity of the bulky Cu fragment, the mixing is improper with the Al matrix. However, due to high heat generation at 1200 rev/min Cu became finer and viscosity increases which helps to bond with Al for both without alloying and with Zn allowing cases. The observed voids may be due to inadequate heat generation. It is also observed that more heat can create local thinning with insufficient material leading to secondary

voids. The heat input to the plasticized material is almost invariable above certain tool rotational speed leading to proper joint. However, in some cases, improper joints arise due to less heat generation below a certain tool rotational speed. At excessively high tool rotational speed (at 2400 rev/min) varies high amount of heat is generated at the nugget area. Due to excess heat, voids are also formed and the bonding looks like hook bond between Al and Cu as shown in Fig. 4g. However, at the same tool rotation speed, some amount of heat is compensated by the extra added Zn alloying element and void is minimized as shown in the Fig. 4h.

### 3.4 Microstructural evolution

Weld bead microstructure has a critical effect on the joint quality. So, a careful investigation of the microstructure of welded samples is needed. The specimens E2 and EZn2 give best weld strength, for without and with alloying element, respectively, as mentioned in Sect. 3.2. Figure 5 shows that the NZ grain size of Al side (44  $\mu\text{m}$ ) is finer compared to the thermo-mechanically affected zone (TMAZ) (59  $\mu\text{m}$ ). The material in the NZ is stirred by the rotating pin, whereas TMAZ is affected only by the shoulder of the tool [19, 20]. Similar result is also observed towards the Cu side. It was detected that the NZ bears finer grains (43  $\mu\text{m}$ ) compared to the TMAZ (64  $\mu\text{m}$ ). Using the same process parameter setting, finer microstructure was obtained for the case of Zn alloying at the weld zone. In Fig. 5b, it is observed that the grain sizes at Al side of NZ and TMAZ with Zn alloying element are 35  $\mu\text{m}$  and 50  $\mu\text{m}$ , respectively, which are around 20% and 15% finer than without

alloying. The NZ grain size is 62% finer than the Al base material (93  $\mu\text{m}$ ). Similarly, on the Cu side, it was observed that the NZ grain is 38  $\mu\text{m}$  and TMAZ grain is 55  $\mu\text{m}$  which are 12% and 14% finer compared to without Zn alloying. The NZ grain of Cu side is 83% finer compared to the Cu base material (229  $\mu\text{m}$ ).

### 3.5 Effect of solid solution phase constituent

Analysis of phase constituents is necessary for the identification of different IMCs and individual percentage of different constituent elements at the weld nugget. The formed phase constituents are detected using line scan, mapping, XRD and EDX technique. From the ultimate tensile strength result (Sect. 3.2), it is observed that the experiment Nos. E2 without alloying and EZn2 with Zn alloying give best tensile strength. So, in this section a detailed investigation is represented to relate the effect of phase

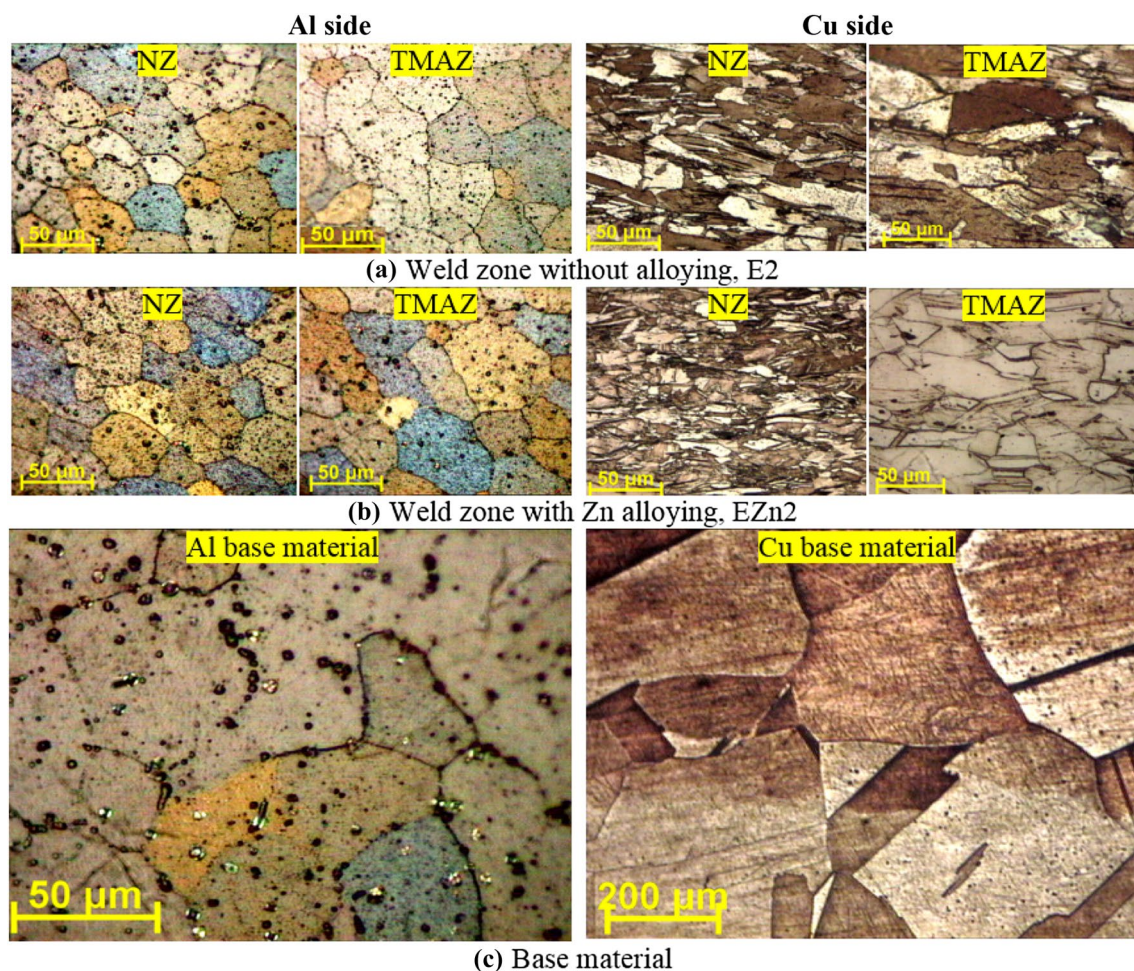


**Fig. 5** Microstructural variation at TMAZ and NZ of **a** without alloying of specimen E2, **b** with Zn alloying element of specimen EZn2 and **c** base materials microstructure

constituents on the metallurgical and mechanical properties of the experiments E2 and EZn2.

### 3.5.1 Line scan and mapping at the weld nugget

Line scan and mapping of the NZ cross-section is one of the methods to detect the phase constitution. The phase in the form of flow pattern can be detected using line scan technique and individual element distribution can be detected by the mapping technique. Line scan and

mapping at the nugget in non-alloying as well as alloying with Zn are given in the Fig. 6a–d, respectively. Both the mapping as well as line scan was achieved in the same area. In the line scan image, Fig. 6a, the red line is indicating the Cu and the green line indicates the Al alloy distribution of sample E2. The zigzag and non-uniform pattern of the line scan indicates the formation of IMCs and its distribution. It is detected that the intensity of Al is higher than the Cu which indicates bulk distribution of the Cu element on the Al matrix. The mapping as shown in the

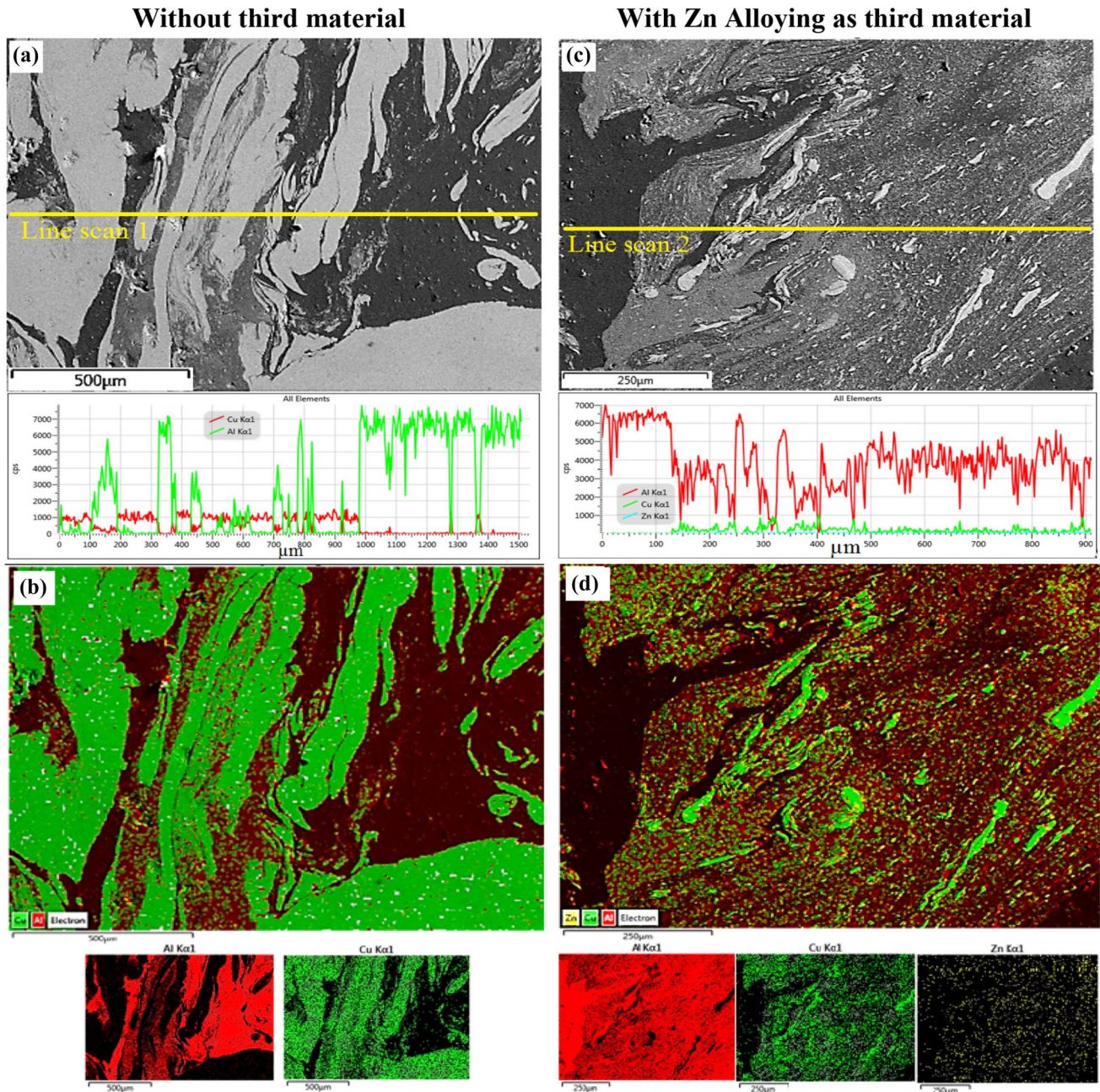


**Fig. 6** Line scan and element mapping of weld nugget **a, b** specimen without alloying, E2 and **c, d** specimen with Zn alloying, EZn2



Fig. 6b indicates that the distribution pattern of Cu particles is uniform over the Al matrix. So, it is confirmed that the NZ consists of Al-Cu binary phase. And the exact phase constituents' names can be identified by XRD technique and can be compared with EDX analysis. A thin layer by layer uniform and uninterrupted IMCs are distributed over the NZ. It was detected that the intensity of Al is more due to offsetting of tool toward the Al side during the experiment.

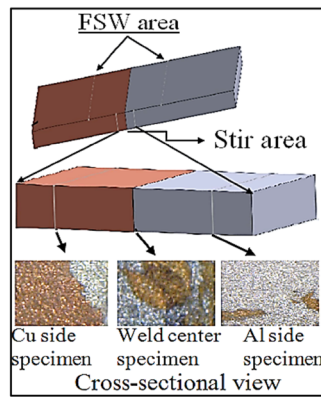
The line scan/mapping of welded sample with Zn inter-layer alloying is relatively dissimilar compare to the non-alloying case. In the line scan image, Fig. 6c, the red line is indicating the Al and the green line indicates the Cu alloy distribution of sample EZn2. The Zn acts as an extra enucleating agent and the IMCs became finer as shown in the Fig. 6c, d compared to without alloying. It is observed that Al intensity is higher and its act as a matrix to the substrate. It is also detected that Zn element mixed with the Al and Cu and distributed throughout the NZ in the form of binary and ternary IMCs. The zigzag pattern indicates uniform mixing of Zn particles in the nugget zone most likely in the form of binary and ternary IMCs. The mapping of Al/Cu with Zn element is represented in Fig. 6d and the corresponding image shows its individual elemental distribution. It was witnessed that the generated IMCs are finer and evenly distributed compared to the sample E2. The Zn alloying elements act as nucleation particles which results in formation of finer IMCs in the micron level. The thickness of binary and ternary IMCs is less than 1  $\mu\text{m}$  which are uniformly distributed with laminar arrangement that results the maximum tensile strength (tensile properties is discussed in the Sect. 3.2). The existence of thin, uniform and uninterrupted IMCs are helpful for strong dissimilar bonding [9] which is also observed in this research work in the case of welding with the Zn alloying element. The welding without Zn alloying shows thick IMCs and it would cause formation of brittle IMCs at the joint interface that leads to quick crack formation and propagation resulting in less tensile strength.

### 3.5.2 XRD analysis at the joint cross-section

The presence of IMCs can be found using the XRD analysis and could be compared with EDX analysis. The XRD examination was performed at the nugget of specimens EZn2 (i.e. sample welded using the Zn alloying element) and E2 (sample welded without alloying element). The sub-specimens were extracted from the midpoint of the NZ as well as 2 mm towards the Al side (retreating side) from the weld center and another one at 2 mm towards the Cu side (advancing side) as depicted in Fig. 7a. The different sub-specimens may indicate different IMCs formation. Figure 7b represents the XRD analysis of

specimen E2. Researchers [4] revealed that in dissimilar Al/Cu welding, rich Al phase constitution  $\text{Al}_2\text{Cu}$  formed towards the Al side and rich Cu phase constitution  $\text{Al}_4\text{Cu}_9$  formed at the Cu side. Similar observation is also made in this research work with some other phase constitution in each side. It is depicted in the Fig. 7b that the rich Al phase constituent (2 AlCu peaks and 2  $\text{Al}_2\text{Cu}$  peaks) are detected in the Al side. It also indicates (Fig. 7d) that the presence of Al and Cu in this region are 95% Al and 5%, respectively. The  $\text{Al}_2\text{Cu}$  eutectic phase was formed easily because of higher diffusion property of Cu in Al than Al in Cu [2] as well as presence of high percentage of Al alloy. In the Cu side, 4 peaks of  $\text{Cu}_9\text{Al}_4$ , 1 peak of AlCu and 2  $\text{Al}_2\text{Cu}_3$  peaks are dominated with overall 90% Cu and 10% Al. At the Cu side, the dominating phase is  $\text{Cu}_9\text{Al}_4$  because of low diffusivity of Al in Cu crystal [2]. However, the center of the weld nugget contains around 54% Al and 46% Cu, as shown in the Fig. 7d, with 6 peaks of AlCu and 1 peak of  $\text{Al}_2\text{Cu}$ . Similar type of IMCs is also detected by other researchers [21–23] due to Al/Cu reaction.

Zn alloy is a highly reactive element and possesses a high rate of diffusion [7, 24] with the Al and Cu to form different phase constituents which are beneficial in strengthening the weld. Zn element can easily melt (melting point is 419.5  $^\circ\text{C}$ ) at the generated process temperature (around 520  $^\circ\text{C}$ ). The XRD study of sample EZn2 is presented in the Fig. 7c. Similar to the previous case, Al side is having 3 peaks of pure Al, 1 peak of pure Zn and 3 peaks of  $\text{Al}_{.71}\text{Zn}_{.29}$  phase constitution. The percentage elemental distributions are 69% Al, 26% Cu and 5% Zn, as shown in Fig. 7e. It was also detected that the  $\text{Al}_{.71}\text{Zn}_{.29}$  phase intensity is higher compared to the pure Al and Cu which indicates high percentage of IMCs formation than the pure Al and Zn. The formation of large amounts of  $\text{Al}_{.71}\text{Zn}_{.29}$  phase is due to low melting, high rate of diffusion and easy reaction of Zn with Al and Cu element. However, at the Cu side, 1 peak each of  $\text{Al}_{.71}\text{Zn}_{.29}$ ,  $\text{CuZn}_5$ , and  $\text{Al}_{4.2}\text{Cu}_{3.2}\text{Zn}_{.7}$  phase constituents at higher intensity than 2 peaks unreacted Cu and 1 peak of Zn were found. The  $\text{CuZn}_5$  forms easily at low temperature (around 425  $^\circ\text{C}$ ) compared to the other phases [2]. The center of the nugget is having 2 peaks of  $\text{Al}_{4.2}\text{Cu}_{3.2}\text{Zn}_{.7}$ , 3 peaks of  $\text{Al}_{.71}\text{Zn}_{.29}$ , 1 peak of  $\text{CuZn}_5$  with 1 peak each of pure Cu, Al and Zn at less intensity compared to the binary and ternary phase constituents. The percentage effect shows 54% Al, 36% Cu and 10% Zn. The  $\text{CuZn}_5$  phase constituent helps in compensating the formation of unfavorable  $\text{Al}_2\text{Cu}$  compound [2] and enhances the tensile strength. The formed eutectic  $\text{Al}_2\text{Cu}$  deteriorates the mechanical properties [2]. It is also observed that thin and more uniform distribution of IMCs in case of EZn2 specimen increased the tensile strength compared to E2.



(a) Schematic of the specimen extraction for XRD analysis

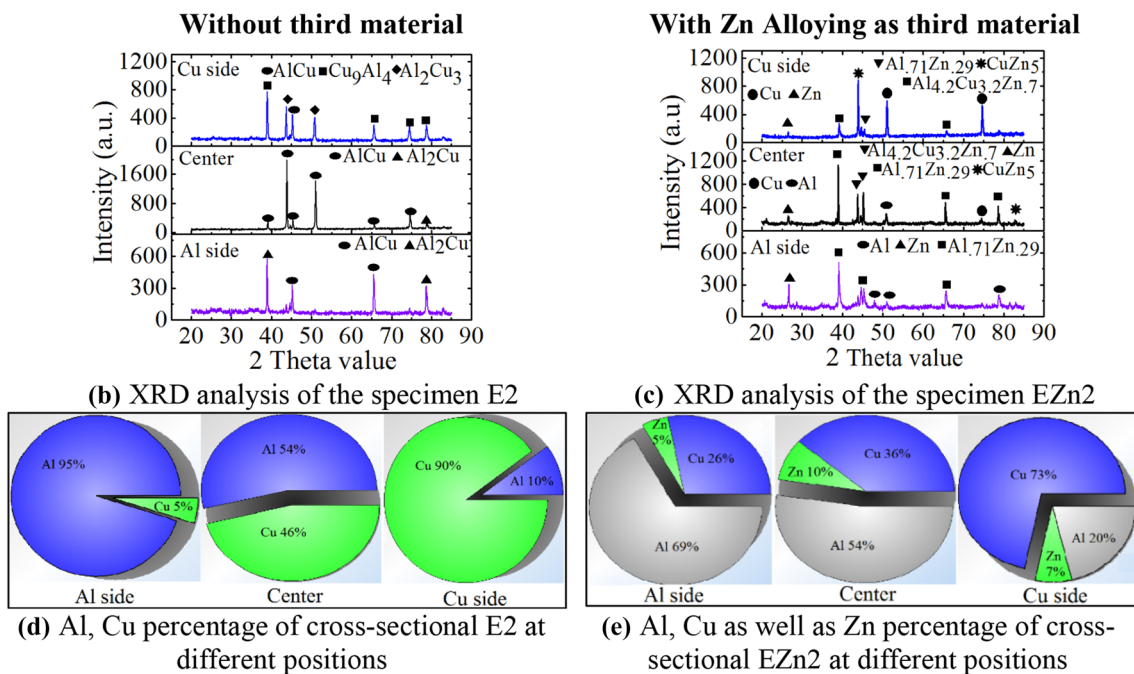


Fig. 7 XRD analysis of specimens E2 and EZn2

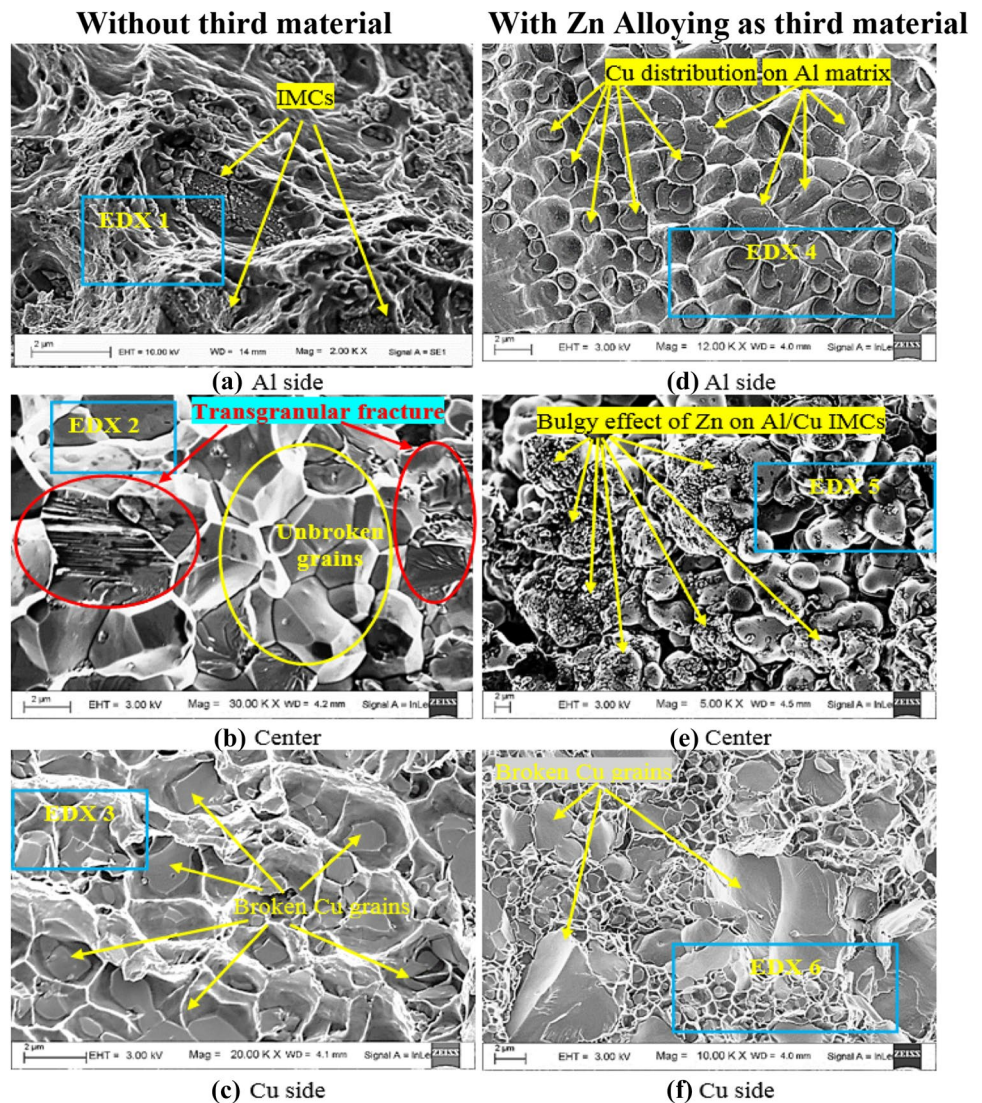
### 3.5.3 Fractography of fractured surface and EDX analysis

Fractography was performed for all tensile tested specimens at the fractured area and the results of selected fracture specimens of E2-4 and EZn2-4 are presented and compared with the XRD analysis, discussed in the Sect. 3.5.2. To compare with the XRD analysis, the fractograph was also performed for specimens which were fractured at the Al side of the NZ, center of the NZ and at the Cu side of the NZ as shown in Fig. 2a. The fractograph and corresponding EDX examination of fractured part of E2-4 and EZn2-4 specimens are characterized in the Figs. 8 and 9. The fractograph indicates that the fracture is not purely ductile. It is a mixture of ductile and brittle

fracture due to the presence of different phase constituents and the IMCs.

Figure 8a represents the fractograph of specimen E2, which was welded without using Zn as alloying element. This sample fractures at the NZ/TMAZ interface towards the Al side with better tensile strength. The fractograph indicates that the fracture is not purely ductile fracture due to the presence of AlCu and Al<sub>2</sub>Cu phase constituents as observed by the XRD analysis. The EDX analysis of the same specimen (EDX 1), as shown in the Fig. 9a, represents 95.8% Al and 4.2% Cu which is quite similar to the XRD analysis of Al side sample as represented in the Fig. 7d. The specimen E3 as represented in Fig. 8b broke at the NZ. The fractograph surface indicates transgranular fracture

**Fig. 8** FESEM images of fractograph of **a–c** specimens E2, E3 and E4 respectively, **d–f** specimens EZn2, EZn3 and EZn4 respectively



in one crystal plane and the other crystal plane consists of unbroken, complete grain as shown in the Fig. 8b. The individual broken grain indicates transgranular fracture as shown inside the oval shape of Fig. 8b. The source of fracture initiated at the NZ and propagated towards the TMAZ and the grains, which come in this fractured zone, broke in transgranular manner. EDX 2 as shown in the Fig. 9b represents around 50% Al and Cu which is also quite similar to the XRD analysis. It indicates that the main phase constituent in this area is AlCu [13, 21] which was also detected by the XRD analysis. But in case of E4 the fracture occurs at Cu side as represented in the Fig. 8c. However, in case of Cu side, 88% Cu is present in the form of  $\text{Cu}_9\text{Al}_4$  and  $\text{Al}_2\text{Cu}_3$  IMCs [13, 21] as shown in the Fig. 9c. It is also well agreed with the XRD analysis. The fracture, as shown in the Fig. 8c, indicates a mixture of ductile and brittle fracture with feather markings, cleavage facets, river patterns and transgranular Cu grain.

When considering the fractograph in case of Zn alloying, it was detected that the fracture happened at the NZ/TMAZ boundary of the Al side in case of EZn2 as shown in the Fig. 8d. The figure indicates dispersed particles of Cu in the dimples of Al matrix initiating the occurrence of tearing. It was also observed that the distribution of fine Cu particles is uniform with regular dimple which helps in maximum strengthening the weld joint. The EDX analysis in this area, as shown in the Fig. 9d, indicates 3.1% Zn which is quite similar to XRD analysis and it forms  $\text{Al}_{71}\text{Zn}_{29}$  phase constituent to strengthen the weld. However, the fractured surface at the center of NZ is quite different from the previous case in case of EZn3 as shown in the Fig. 8e. It was detected that Al/Cu IMCs are covered by fine Zn particles, as revealed in Fig. 8e, which provides additional strengthening effect compared to E3 and gives highest tensile strength. The fractured surface shows bulge grains that are

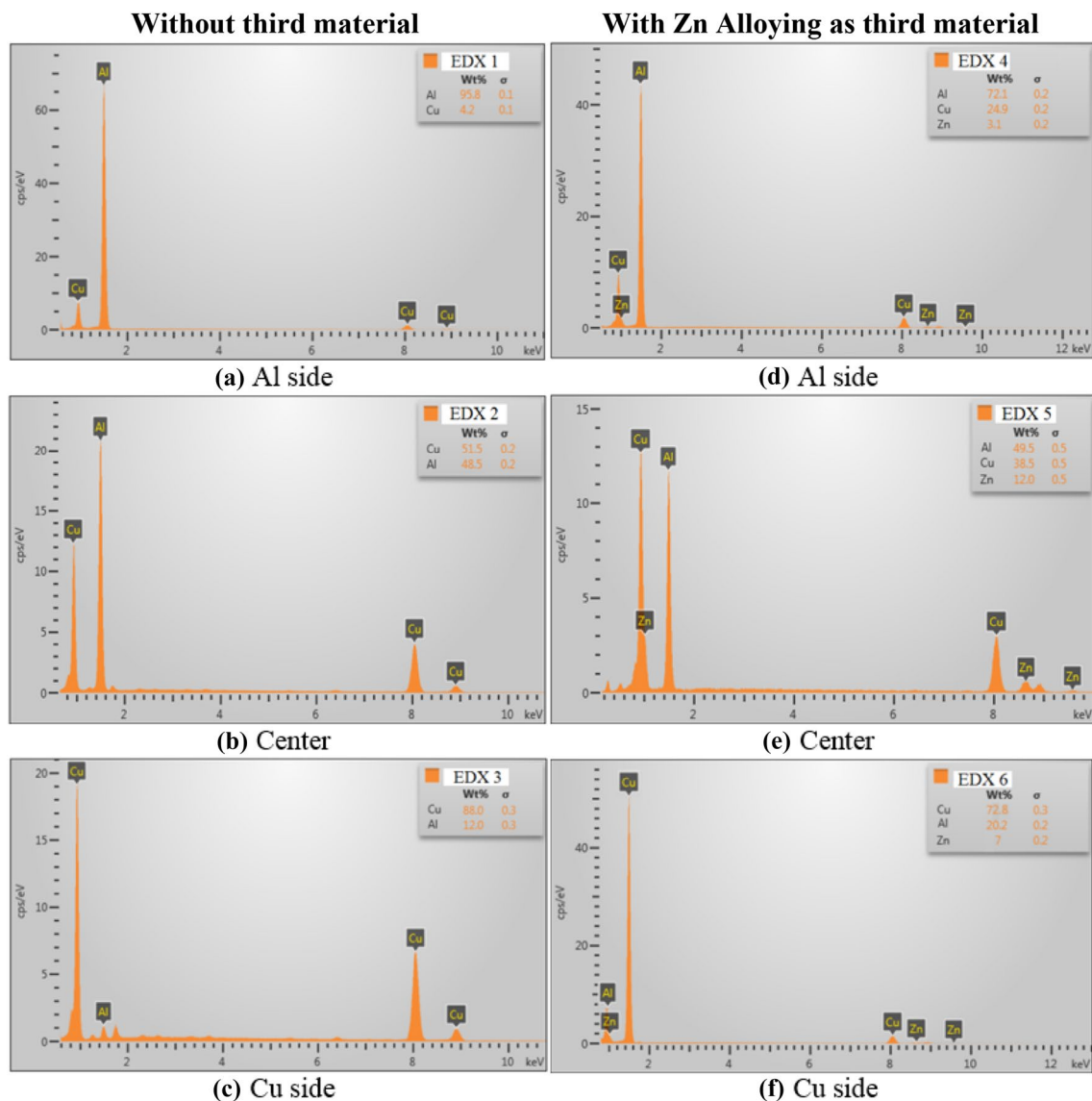


**Fig. 9** FESEM-EDX analysis at Al side, center and Cu side of the nugget of **a–c** specimens E2, E3 and E4 respectively, **d–f** specimens EZn2, EZn3 and EZn4 respectively

accumulated by some Zn alloying third material owing to proper melting of Zn at the NZ. The EDX analysis in this area is showing around 12% Zn, as shown in the Fig. 9e, and it is higher than the other cases and also similar to the observation by XRD analysis with formation of CuZn<sub>5</sub> phase constituent. But, at the Cu side of the NZ fracture indicates 7% Zn as shown in the Fig. 9f by the EDX analysis with the formation of Al<sub>71</sub>Zn<sub>29</sub>, CuZn<sub>5</sub> and Al<sub>4.2</sub>Cu<sub>3.2</sub>Zn<sub>7</sub> phase constituents. The fractograph as shown in the Fig. 8f represents transgranular fracture, sharp edges, and cleavage planes with atomic steps designating brittle fracture owing to formation of different binary and ternary IMCs that deteriorated the strength of EZn4 sample.

### 4 Conclusions

The aforementioned experimental results can be concluded as follows:

- Phase constituents play an effective role to achieve successful joint with sound mechanical and metallurgical properties.
- The weld surface and bead geometry analysis indicate non-defective weld with good surface appearance and uniform flow mark below the tool shoulder at tool rotation speed of 1200 rev/min for both non-alloying and alloying cases.

- Macrostructural and material flow analysis reveals that in case of Zn alloying, the weld cross-section has less defects with finer IMCs at the NZ. The microstructural analysis indicates finest grains at the NZ due to the nucleating effect of the Zn alloying element.
- The formed fine and uniformly distributed binary and ternary phase constituents like  $Al_{.71}Zn_{.29}$ ,  $Al_{4.2}Cu_{3.2}Zn_{.7}$  and  $CuZn_3$  are acting as strengthening IMCs to attain best metallurgical and mechanical properties.
- The line scan and mapping reveal the formation of micron level IMCs which strengthen the weld quality. Both the XRD analysis and EDX analysis reveal similar binary and ternary phase constitutions in the weld bead.
- The fractograph indicates transgranular fracture with broken and complete 3D grain at the NZ. The fracture initiated at the NZ and propagated towards the TMAZ.
- The mechanical tests reveal that maximum tensile strength in Zn alloying is increased by 13% compared to non-alloying case and 108% of the Al base material. The micro-hardness of the weld nugget also increases because of the formation of thin, uniform and controlled binary and ternary IMCs at the NZ.

**Acknowledgements** The present research work was supported by Mechanical Engineering Department and Central Instruments Facility, IIT Guwahati for providing experimental facility and conduct testing.

### Compliance with ethical standards

**Conflict of interest** The authors declare that they have no conflict of interest.

### References

1. Akbari M, Bahemmat P, Haghpanahi M, Givi MKB (2013) Enhancing metallurgical and mechanical properties of friction stir lap welding of Al–Cu using intermediate layer. *Sci Technol Weld Join* 18(6):518–524
2. Balasundaram R, Patel VK, Bhole SD, Chen DL (2014) Effect of zinc interlayer on ultrasonic spot welded aluminum to copper joints. *Mater Sci Eng, A* 607:277–286
3. Kuang B, Shen Y, Chen W, Yao X, Xu H, Gao J, Zhang J (2015) The dissimilar friction stir lap welding of 1A99 Al to pure Cu using Zn as filler metal with pinless tool configuration. *Mater Des* 68:54–62
4. Xue P, Xiao BL, Ni DR, Ma ZY (2010) Enhanced mechanical properties of friction stir welded dissimilar Al–Cu joint by intermetallic compounds. *Mater Sci Eng, A* 527:5723–5727
5. Boucherit A, Avettand-Fenoel MN, Taillard R (2017) Effect of a Zn interlayer on dissimilar FSSW of Al and Cu. *Mater Des* 124:87–99
6. Kandasamy J, Hussain MM, Rajesham S (2012) Heterogeneous friction stir welding: improved properties in dissimilar aluminum alloy joints through insertion of copper coupled with external heating. *Mater Manuf Process* 27:1429–1436
7. Shiri SG, Sarani A, Hosseini SRE, Roudini G (2013) Diffusion in FSW joints by inserting the metallic foils. *J Mater Sci Technol* 29(11):1091–1095
8. Aonuma M, Nakata K (2009) Effect of alloying elements on interface microstructure of Mg–Al–Zn magnesium alloys and titanium joint by friction stir welding. *Mater Sci Eng, B* 161:46–49
9. Aonuma M, Nakata K (2010) Effect of calcium on intermetallic compound layer at interface of calcium added magnesium–aluminum alloy and titanium joint by friction stir welding. *Mater Sci Eng, B* 173:135–138
10. Zheng Q, Feng X, Shen Y, Huang G, Zhao P (2016) Dissimilar friction stir welding of 6061 Al to 316 stainless steel using Zn as a filler metal. *J Alloy Compd* 686:693–701
11. Ratanathavorn W, Melander A (2017) Influence of zinc on intermetallic compounds formed in friction stir welding of AA5754 aluminium alloy to galvanized ultra-high strength steel. *Sci Technol Weld Join* 22(8):673–680
12. Handbook ASM (1992) Alloy phase diagrams, vol 3. ASM International, Cleveland
13. Sahu PK, Pal S, Pal SK, Jain R (2016) Influence of plate position, tool offset and tool rotational speed on mechanical properties and microstructures of dissimilar Al/Cu friction stir welding joints. *J Mater Process Technol* 235:55–67
14. Al-Roubaiy AO, Nabat SM, Batako ADL (2014) Experimental and theoretical analysis of friction stir welding of Al–Cu joints. *Int J Adv Manuf Technol* 71:1631–1642
15. Zhang J, Luo G, Wang Y, Xiao Y, Shen Q, Zhang L (2013) Effect of Al thin film and Ni foil interlayer on diffusion bonded Mg–Al dissimilar joints. *J Alloy Compd* 556:139–142
16. Hsu CJ, Chang CY, Kao PW, Ho NJ, Chang CP (2006) Al–Al<sub>3</sub>Ti nanocomposites produced in situ by friction stir processing. *Acta Mater* 54:5241–5249
17. Sahu PK, Pal S (2017) Influence of metallic foil alloying by FSW process on mechanical properties and metallurgical characterization of AM20 Mg alloy. *Mater Sci Eng, A* 684:442–455
18. Sahu PK, Pal S (2018) Effect of FSW parameters on microstructure and mechanical properties of AM20 welds. *Mater Manuf Process* 33:288–298
19. Sahu PK, Kumari K, Pal S, Pal SK (2016) Hybrid fuzzy-grey-Taguchi based multi weld quality optimization of Al/Cu dissimilar friction stir welded joints. *Adv Manuf* 4:237–247
20. Sahu PK, Pal S (2017) Mechanical properties of dissimilar thickness aluminium alloy weld by single/double pass FSW. *J Mater Process Technol* 243:442–455
21. Tan CW, Jiang ZG, Li LQ, Chen YB, Chen XY (2013) Microstructural evolution and mechanical properties of dissimilar Al–Cu joints produced by friction stir welding. *Mater Des* 51:466–473
22. Zhang W, Shen Y, Yan Y, Guo R (2017) Dissimilar friction stir welding of 6061 Al to T2 pure Cu adopting tooth shaped joint configuration: microstructure and mechanical properties. *Mater Sci Eng, A* 690:355–364
23. Khojastehnezhad VM, Pourasl HH (2018) Microstructural characterization and mechanical properties of aluminum 6061-T6 plates welded with copper insert plate (Al/Cu/Al) using friction stir welding. *Trans Nonferrous Met Soc China* 28:415–426
24. Grammatikakis J, Eftaxias K, Hadjicontis V (1988) Interconnection of the diffusion coefficients of various elements in aluminum. *J Phys Chem Solids* 49(10):1275–1277

**Publisher's Note** Springer Nature remains neutral with regard to jurisdictional claims in published maps and institutional affiliations.